Radiation pattern of a focused transducer: A numerically convergent solution

Xucai Chen
Rochester Center for Biomedical Ultrasound and Departments of Medicine and Electrical Engineering, University of Rochester, Rochester, New York 14627

Karl Q. Schwarz
Rochester Center for Biomedical Ultrasound and Department of Medicine, University of Rochester, Rochester, New York 14627

Kevin J. Parker
Rochester Center for Biomedical Ultrasound and Department of Electrical Engineering, University of Rochester, Rochester, New York 14627

(Received 17 May 1993; accepted for publication 20 July 1993)

The radiation pattern of a focused transducer is reexamined. The radiation field is divided into an illuminated zone and a shadow zone. A numerically convergent solution of the pressure distribution in terms summations of Bessel functions is provided. This solution is computationally more advantageous than earlier results where a double or single integral in the complex plane is required. The pressure amplitude differs from earlier reports slightly for off-axis locations at low frequency. This difference may have significance for backscatter coefficient determination where scatterers are assumed present over a time-gated volume. The solution for a flat disk radiator is obtained as a limiting case.

PACS numbers: 43.20.Rz, 43.20.Tb, 43.20.Ye, 43.88.Yn

LIST OF SYMBOLS

a	radius of the active transducer element
c	speed of sound in the medium
f	acoustic frequency
G_p	focusing factor of a focused transducer
i	$\sqrt{-1}$, unit of imaginary number
$I(Y,Z)$	Eq. (16)
$J_n(\cdot)$	cylindrical Bessel function of order n, and argument $(\cdot)$
k	wave number
$p(r,\theta)$	pressure distribution
$p'(r,\theta)$	normalized pressure distribution
p_0	pressure amplitude on the transducer surface
P	total transmitted acoustic power
r	the distance from the center of the transducer to the observation point
r'	the distance from the point source on the transducer to the observation point
r_0	the radius of curvature
r_1	the distance from the focus of the transducer to the observation point
t	time variable
u	dummy variable for integration
u_0	the normal velocity amplitude on the transducer surface
u_1, u_2	first- and second-order Lommel functions of the first kind, Eq. (19)
u_1', u_2'	Eq. (23)
v_0, v_1	zeroth- and first-order Lommel function of the first kind, Eq. (30)
w	distance from the focal point along the boundary line
x	radial distance from the acoustic axis
x_n, x'_n	location of pressure nodes in the focal plane
Y,Z	normalized position of the observation point, Eq. (15)
Y',Z'	normalized position of the observation point, Eq. (82)
z	axial distance from the center of transducer along the acoustic axis
z_{1n}	roots of $J_1(z)$
z_n, z'_n	location of pressure nodes along the axis
α	the half-aperture angle
ε	truncation error
θ	polar angle of the observation point
θ_0	polar angle of the point source relative to the focus of the transducer
θ_1	polar angle of the observation point relative to the focus of the transducer
φ_0	azimuthal angle of the point source relative to the focus of the transducer
ϕ	the velocity potential
ρ_0	density of the medium
ω	angular frequency

 0001-4966/93/94(5)/2979/13/$6.00

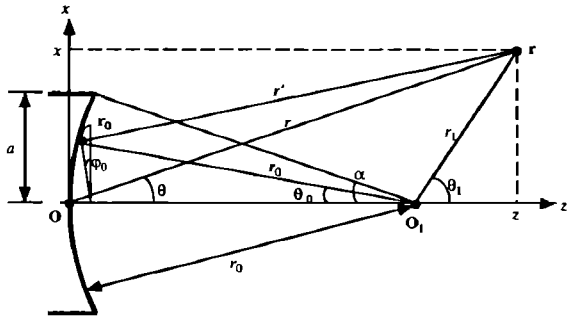

FIG. 1. Coordinate systems used for analysis.

INTRODUCTION

The radiation pattern of a flat or focused radiator has been studied by many authors. For a flat circular transducer, the radiation pattern is found by direct integration of the Green's function over the face of the transducer, as formulated by Rayleigh. This double integration has been reduced to a single integration by Stepanishen[1] and Lockwood and Willette.[2] For a focused transducer, the Rayleigh formula is only an approximation, and this approximation is good if the radius of the transducer is larger than the wavelength, as O'Neil[3] has pointed out. O'Neil stated that the general expression for the off-axis intensity distribution is complicated and requires the evaluation of a double integral. Penttinen and Luukkala,[4] Madsen *et al.*,[5] and later Lucas and Muir[6] reduced the solution to a single integral. In the solution by Lucas and Muir,[6] the Fresnel approximation is used to transform the boundary condition on the curved surface into a boundary condition at the $z=0$ plane. The Helmholtz equation is transformed into a parabolic equation by using the parabolic approximation. Their solution was later expressed in a series solution by Cobb.[7]

A numerically convergent solution for the pressure distribution of the focused transducer is presented in this communication. In Sec. I, a single-integral solution of the pressured distribution of a focused transducer is derived directly from the Rayleigh formulation. In Sec. II this solution is reduced to a summation in terms of cylindrical Bessel functions by using the Lommel integrals. Alternative solutions are provided for different zones of the pressure field such that the summation converges everywhere in the right half-space where the pressure distribution is desired. Graphical presentation and discussion of the solution is given in Sec. III. The pressure distribution of a flat transducer in terms of cylindrical Bessel functions is provided as a limiting case of the focused transducer in Sec. IV. Some numerical considerations are given in Sec. V.

I. A SINGLE-INTEGRAL SOLUTION OF THE PRESSURE DISTRIBUTION

The geometry of the focused transducer is shown in Fig. 1. The half-aperture angle, α, is determined by the radius of the transducer and the radius of curvature as

$$\alpha=\arcsin a/r_0. \tag{1}$$

When the size of the transducer is larger than the acoustic wavelength ($ka>1$), the velocity potential in the right half-space can be calculated by the Green's function method (the Rayleigh formulation):

$$\phi(r,\theta)=\frac{u_0}{2\pi}\int\int_S \frac{\exp(-ikr')}{r'}\,dS, \tag{2}$$

where u_0 is the normal velocity on the transducer face, r' is the distance from a point source on the surface of the transducer to the point of observation, and integration is over the whole surface of the transducer. The time dependence, $\exp(i\omega t)$, has been suppressed. The solution is axis symmetric so either polar or cylindrical coordinate system can be used. The polar coordinate system with its origin located at the center of the transducer will be used in our derivation. The distance r', however, is best described by a spherical coordinate system with its origin O_1 located at the geometrical focus of the transducer, as shown in Fig. 1. Then the observation point $\mathbf{r}(r,\theta)$ can be expressed as $(r_1,\theta_1,0)$ in the new coordinate system where

$$\begin{aligned} r\cos\theta&=r_1\cos\theta_1+r_0,\\ r\sin\theta&=r_1\sin\theta_1. \end{aligned} \tag{3}$$

A point on the transducer surface can be expressed as (r_0,θ_0,φ_0). Then

$$r'=[r_1^2+r_0^2+2r_1r_0(\cos\theta_1\cos\theta_0 -\sin\theta_1\sin\theta_0\cos\varphi_0)]^{1/2}. \tag{4}$$

Eliminating r_1 and θ_1 from Eqs. (3) and (4), we find

$$r'=\left\{r^2+2r_0^2\left[\left(1-\frac{r\cos\theta}{r_0}\right)(1-\cos\theta_0) -\frac{r\sin\theta}{r_0}\sin\theta_0\cos\varphi_0\right]\right\}^{1/2}. \tag{5}$$

Assuming that r' in the exponent of Eq. (2) can be replaced by the first two terms of its bimodal expansion,

$$r'=r+\frac{r_0^2}{r}\left[\left(1-\frac{r\cos\theta}{r_0}\right)(1-\cos\theta_0) -\frac{r\sin\theta}{r_0}\sin\theta_0\cos\varphi_0\right]+\cdots, \tag{6}$$

and r' in the denominator can be replaced by r (the Fresnel approximation), then

$$\phi(r,\theta)=\frac{u_0r_0^2}{2\pi r}\exp(-ikr)\int_{\theta_0=0}^{\alpha}\exp\left[-i\frac{kr_0^2}{r} \times\left(1-\frac{r}{r_0}\cos\theta\right)(1-\cos\theta_0)\right]\sin\theta_0\,d\theta_0 * \int_{\varphi_0=0}^{2\pi}\exp(ikr_0\sin\theta_1\sin\theta_0\cos\varphi_0)\,d\varphi_0, \tag{7}$$

where $dS=r_0^2\sin\theta_0\,d\theta_0\,d\varphi_0$ has been used. The integration over φ_0 can be accomplished explicitly to give

$$\phi=\frac{u_0 r_0^2}{r}\exp(-ikr)\int_{\theta_0=0}^{\alpha}\exp\left[-i\frac{kr_0^2}{r}\left(1-\frac{r}{r_0}\cos\theta\right)\right.$$

$$\left.\times(1-\cos\theta_0)\right]\sin\theta_0 * J_0(kr_0\sin\theta\sin\theta_0)d\theta_0. \quad (8)$$

Let $u=(r_0/a)\sin\theta_0$, then

$$1-\cos\theta_0=\frac{1}{2}\left(\frac{a}{r_0}\right)^2 u^2\left[1+\frac{1}{4}\left(\frac{a}{r_0}\right)^2 u^2+\cdots\right]. \quad (9)$$

Keeping the first term of Eq. (7) only and substituting into Eq. (6), we have

$$\phi(r,\theta)=\frac{u_0 a^2}{r}\exp(-ikr)\int_{u=0}^{1}\exp\left[-i\frac{ka^2}{2r}\right.$$

$$\left.\times\left(1-\frac{r}{r_0}\cos\theta\right)u^2\right]uJ_0(ka\sin\theta u)du. \quad (10)$$

Equation (10) is the integral solution of the velocity potential in the polar coordinate system.

The acoustic pressure can be derived from the velocity potential by

$$p(r,\theta)=i\rho_0\frac{\partial\phi(r,\theta)}{\partial t}=i\rho_0\omega\phi(r,\theta). \quad (11)$$

Define

$$p_0\equiv\rho_0 c u_0, \quad (12)$$

which will be shown later as the power equivalent pressure amplitude on the transducer surface, then

$$p(r,\theta)=i(p_0/u_0)k\phi(r,\theta). \quad (13)$$

Substituting Eq. (10) into Eq. (13), we obtain the pressure distribution of the focused transducer as,

$$p(r,\theta)=ip_0\frac{ka^2}{r}\exp(-ikr)\int_{u=0}^{1}\exp\left[-i\frac{ka^2}{2r}\right.$$

$$\left.\times\left(1-\frac{r}{r_0}\cos\theta\right)u^2\right]uJ_0(ka\sin\theta u)du. \quad (14)$$

From now on we will only discuss the pressure distribution given in Eq. (14).

II. SERIES SOLUTIONS IN TERMS OF BESSEL FUNCTIONS

The solution given in Eq. (14) can be transformed into a series solution by using the Lommel integrals. Define

$$Y=(ka^2/r)[1-(r/r_0)\cos\theta],$$
$$Z=ka\sin\theta, \quad (15)$$

and

$$I(Y,Z)=Y\int_{u=0}^{1}\exp\left(-i\frac{Y}{2}u^2\right)uJ_0(Zu)du, \quad (16)$$

then Eq. (14) is reduced to

$$p(r,\theta)=\frac{ip_0\exp(-ikr)}{1-r\cos\theta/r_0}I(Y,Z). \quad (17)$$

The two-parameter problem similar to that given in Eq. (16) has been discussed in detail by Lommel.[8] The following two equations are given (Eq. 32 in Ref. 8):

$$C=\int_{u=0}^{1}\cos\left(\frac{Y}{2}(1-u^2)\right)uJ_0(Zu)du=\frac{1}{Y}u_1(Y,Z),$$
$$S=\int_{u=0}^{1}\sin\left(\frac{Y}{2}(1-u^2)\right)uJ_0(Zu)du=\frac{1}{Y}u_2(Y,Z), \quad (18)$$

where

$$u_1(Y,Z)=\sum_{n=0}^{\infty}(-1)^n\left(\frac{Y}{Z}\right)^{2n+1}J_{2n+1}(Z),$$
$$u_2(Y,Z)=\sum_{n=0}^{\infty}(-1)^n\left(\frac{Y}{Z}\right)^{2n+2}J_{2n+2}(Z). \quad (19)$$

These equations can be obtained by repeated use of integration by parts using

$$\int_0^Z Z^n J_{n-1}(Z)dZ=Z^n J_n(Z). \quad (20)$$

Some manipulation of the above equations provides the general solution for Eq. (16) as

$$I(Y,Z)=\exp[-i(Y/2)][u_1(Y,Z)+iu_2(Y,Z)], \quad (21)$$

and its amplitude is given by

$$|I(Y,Z)|=\{[u_1(Y,Z)]^2+[u_2(Y,Z)]^2\}^{1/2}. \quad (22)$$

It is sometimes more advantageous to use

$$u_1'(Y,Z)=\sum_{n=0}^{\infty}(-1)^n\left(\frac{Y}{Z}\right)^{2n}J_{2n+1}(Z),$$
$$u_2'(Y,Z)=\sum_{n=0}^{\infty}(-1)^n\left(\frac{Y}{Z}\right)^{2n+1}J_{2n+2}(Z), \quad (23)$$

then Eq. (21) becomes

$$I(Y,Z)=\exp\left(-i\frac{Y}{2}\right)\frac{Y}{Z}[u_1'(Y,Z)+iu_2'(Y,Z)], \quad (24)$$

The series u_1 and u_2 converges for all values of Y and Z. They may converge slowly, however, for some values of Y and Z. Observing the ratio of $Y/Z=-\sin(\alpha)/\tan(\theta_1)$ with the help of Eq. (3), we find

$$\left|\frac{Y}{Z}\right|=\begin{cases}<1, & \text{shadow zone } (\alpha<\theta_1<\pi-\alpha),\\ =1, & \text{boundary } (\theta_1=\alpha \text{ or } \theta_1=\pi-\alpha),\\ >1, & \text{illuminated zone } (\theta_1<\alpha \text{ or } \theta_1<\pi-\alpha).\end{cases} \quad (25)$$

Depending on the value of θ_1, the radiation field is divided into two zones, the shadow zone and the illuminated zone, as depicted in Fig. 2.

A. Solution for the shadow zone ($\alpha<\theta_1<\pi-\alpha$)

Since $|Y/Z|<1$ for $\alpha<\theta_1<\pi-\alpha$, the series given in Eq. (22) converges uniformly, and Eq. (23) is used directly with Eq. (17) to calculate the pressure distribution in the shadow zone.

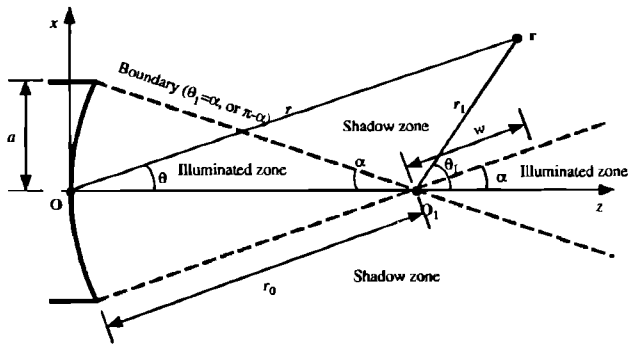

FIG. 2. The definition of illuminated and shadow zones and the boundary line for a focused transducer.

B. Solution on the boundary ($\theta_1=\alpha$ or $\theta_1=\pi-\alpha$)

Since $|Y/Z|=1$ for $\theta_1=\alpha$, or $\theta_1=\pi-\alpha$, the functions in Eq. (22) can be expressed explicitly as

$$u_1(\pm Z,Z)=\pm\sum_{n=0}^{\infty}(-1)^n J_{2n+1}(Z)=\pm\frac{1}{2}\sin(Z), \tag{26}$$

$$u_2(\pm Z,Z)=\sum_{n=0}^{\infty}(-1)^n J_{2n+2}(Z)$$
$$=\tfrac{1}{2}[J_0(Z)-\cos(Z)],$$

Therefore:

$$I(\pm Z,Z)=\exp\left(\frac{\pm iZ}{2}\right)\frac{1-\exp(\mp iZ)J_0(Z)}{2i} \tag{27}$$

and its amplitude is

$$|I(\pm Z,Z)|=\tfrac{1}{2}\{1+[J_0(Z)]^2-2\cos(Z)J_0(Z)\}^{1/2}. \tag{28}$$

C. Solution for the illuminated zone ($\theta_1<\alpha$ or $\theta_1>\pi-\alpha$)

Since $|Y/Z|>1$ for $\theta_1<\alpha$, or $\theta_1>\pi-\alpha$, the series expressed as in Eq. (22) may converge slowly. However, the following identities[8] can be used:

$$u_1(Y,Z)=\sin\left(\frac{Y}{2}+\frac{Z^2}{2Y}\right)-v_1(Y,Z),$$
$$u_2(Y,Z)=-\cos\left(\frac{Y}{2}+\frac{Z^2}{2Y}\right)+v_0(Y,Z), \tag{29}$$

where

$$v_0(Y,Z)=\sum_{n=0}^{\infty}(-1)^n\left(\frac{Z}{Y}\right)^{2n}J_{2n}(Z),$$
$$v_1(Y,Z)=\sum_{n=0}^{\infty}(-1)^n\left(\frac{Z}{Y}\right)^{2n+1}J_{2n+1}(Z). \tag{30}$$

Substituting Eq. (29) into Eq. (17), we have

$$I(Y,Z)=-i\exp\left(\frac{iZ^2}{2Y}\right)\left\{1-\exp\left[-i\left(\frac{Y}{2}+\frac{Z^2}{2Y}\right)\right]\right.$$
$$\left.\times[v_0(Y,Z)+iv_1(Y,Z)]\right\} \tag{31}$$

and its amplitude is

$$|I(Y,Z)|=\left[1+v_0^2+v_1^2-2v_0\cos\left(\frac{Y}{2}+\frac{Z^2}{2Y}\right)\right.$$
$$\left.-2v_1\sin\left(\frac{Y}{2}+\frac{Z^2}{2Y}\right)\right]^{1/2}. \tag{32}$$

Equation (31) is used with Eq. (17) for calculating the pressure distribution in the illuminated zone.

III. GRAPHICAL PRESENTATIONS AND DISCUSSION

Since the pressure distribution depends on the geometry of the transducer and the frequency, it is more convenient to compare the focusing characteristics if the pressure distribution is normalized by the pressure at the focal point. It is easy to observe that at the focal point $Y=0$ and $Z=0$. The pressure at the focus, p_{focus}, can be found from the limiting value of Eqs. (17) and (23) to be

$$p_{\text{focus}}=ip_0G_p\exp(-ikr_0), \tag{33}$$

where

$$G_p\equiv\frac{ka^2}{2r_0}\equiv\frac{ka\sin\alpha}{2} \tag{34}$$

is the focusing factor of the transducer, and the pressure amplitude at the focus is p_0G_p.

The normalized pressure distribution is defined as

$$p'(r,\theta)\equiv p(r,\theta)/p_{\text{focus}}. \tag{35}$$

From Eq. (17) we have

$$p'(r,\theta)=\exp[-ik(r-r_0)]\frac{r_0}{r}\frac{2}{Y}I(Y,Z). \tag{36}$$

A. Pressure distribution in the focal plane

In the focal plane where $\theta_1=\pi/2$, $Y=0$, all but the first term in u_1' vanishes, and $u_2'=0$, therefore

$$\frac{2}{Y}I(0,Z)=\frac{2}{Z}J_1(Z)=\frac{2J_1(ka\sin\theta)}{ka\sin\theta}. \tag{37}$$

So the pressure distribution in the focal plane is

$$p'_{\text{focal}}=\exp\left[-ikr_0\left(\frac{1}{\cos\theta}-1\right)\right]\frac{2J_1(ka\sin\theta)}{ka\tan\theta}, \tag{38}$$

since $r_0/r=\cos\theta$. This solution is identical to that given by O'Neil[3] when $kr_0\gg1$ is assumed. Using cylindrical coordinate system as shown in Fig. 1, $\sin\theta=x/\sqrt{x^2+r_0^2}$, and $\tan\theta=x/r_0$, we have in the focal plane

$$|p'_{\text{focal}}|=\left|\frac{2J_1(ka\sin\theta)}{ka\tan\theta}\right|=\left|\frac{2J_1(kax/\sqrt{x^2+r_0^2})}{kax/r_0}\right|. \tag{39}$$

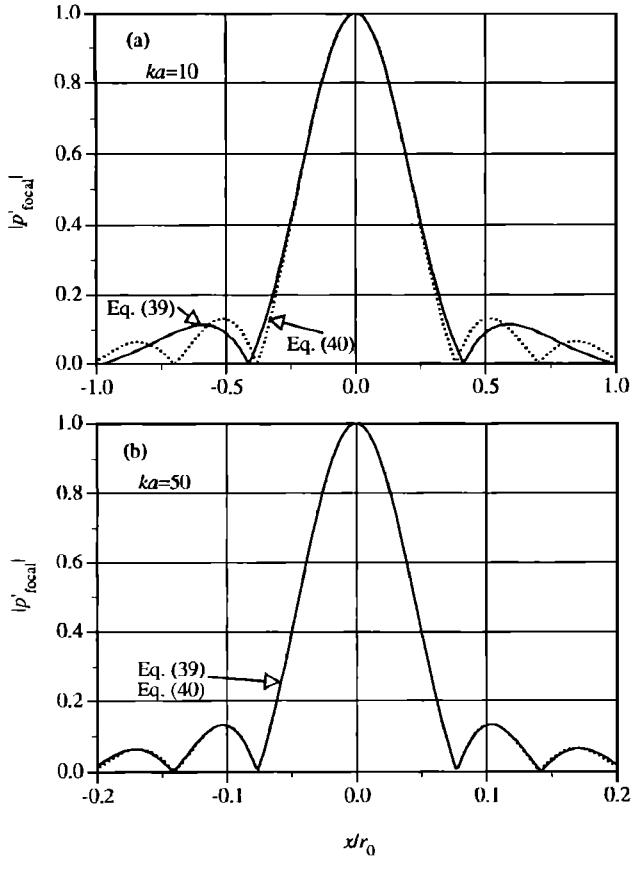

FIG. 3. Normalized pressure distribution in the focal plane of a focused transducer: (a) $\sin\alpha=0.1$, $ka=100$ ($G_p=5$); (b) $\sin\alpha=0.1$, $ka=300$ ($G_p=15$). Dashed lines represent Eq. (40), the solution by Lucas and Muir.

The pressure distribution in the focal plane has also been given by Lucas and Muir[6] as

$$|p'_{\text{Lucas}}|=\left|\frac{2J_1(ka\tan\theta)}{ka\tan\theta}\right|=\left|\frac{2J_1(kax/r_0)}{kax/r_0}\right|. \tag{40}$$

For Eq. (39) there are a limited number of zeros (pressure nodes) in the focal plane and these zeroes are at

$$\frac{x_n}{r_0}=\frac{z_{1n}/ka}{1-(z_{1n}/ka)^2},\quad z_{1n}<ka, \tag{41}$$

where z_{1n} are the zeros of $J_1(z)$. Equation (40), however, has an infinite number of zeroes in the focal plane at

$$\frac{x'_n}{r_0}=\frac{z_{1n}}{ka}, \tag{42}$$

The -3-dB width of the focal spot in the focal plane from Eq. (39) is found to be slightly larger than that given by Eq. (40) for small values of ka, and approaches

$$2W_{-3\text{ dB}}\approx 2(1.616r_0/ka), \tag{43}$$

as given by Eq. (40) for $ka\gg 1$. Shown in Fig. 3 are the numerical values of Eq. (39) as a function of lateral distance x/r_0, together with Eq. (40), for $\sin\alpha=0.1$ and $ka=10$ and 50. The differences between them diminish for larger ka, as can be seen in Fig. 3(b).

B. On the hemispherical surface $r=r_0$

On the hemispherical surface passing through the focal point ($r=r_0$), we find $Y=4G_p\sin^2\theta/2$ and $Y/Z=(a/r_0)\tan\theta/2$. Therefore,

$$u'_1(Y,Z)=\sum_{n=0}^{\infty}(-1)^n\left(\frac{a}{r_0}\tan\frac{\theta}{2}\right)^{2n}J_{2n+1}(ka\sin\theta),$$
$$u'_2(Y,Z)=\sum_{n=0}^{\infty}(-1)^n\left(\frac{a}{r_0}\tan\frac{\theta}{2}\right)^{2n+1}J_{2n+2}(ka\sin\theta). \tag{44}$$

The normalized pressure distribution on this surface is therefore

$$p'_{r=r_0}=\frac{2}{Y}I(Y,Z)=\exp\left(-i2G_p\sin^2\frac{\theta}{2}\right)\frac{2(u'_1+iu'_2)}{ka\sin\theta}, \tag{45}$$

and its amplitude is

$$|p'_{r=r_0}|=\frac{2}{ka\sin\theta}\left[J_1^2(ka\sin\theta)+\left(\frac{a}{r_0}\tan\frac{\theta}{2}\right)^2\right.$$
$$\times[J_2^2(ka\sin\theta)-2J_1(ka\sin\theta)J_3(ka\sin\theta)]$$
$$\left.+O\left[\left(\frac{a}{r_0}\tan\frac{\theta}{2}\right)^4\right]\right]^{1/2}. \tag{46}$$

For $ka\gg 1$, only the first term is significant. This can be explained by the fact that in the main lobe, θ is small ($\theta<3.83/ka$), thus $[(a/r_0)\tan\theta/2]^2<(1.91/kr_0)^2\ll 1$, while outside the main lobe, the functional value of p' is itself small. Numerical investigation indicates that for $ka>1$ and $\sin\alpha<0.2$ the first term in Eq. (46) gives accuracy better than 10^{-3}. For most purposes, it is sufficient to use the first term only:

$$|p'_{r=r_0}|\approx\left|\frac{2J_1(ka\sin\theta)}{ka\sin\theta}\right|. \tag{47}$$

This is identical to the far field angular distribution function for a flat disk transducer. From Eq. (47) the -3-dB angular beam spread is

$$2\alpha_{-3\text{ dB}}=2\arcsin(1.616/ka). \tag{48}$$

Figure 4 shows the angular distribution on $r=r_0$, Eqs. (46) and (47), for $\sin\alpha=0.1$ and $ka=100$. For these parameters, the difference between them is much smaller than 10^{-3}. From Eqs. (39) and (47), the pressure distribution in the focal plane can be treated as the projection of the angular distribution onto the focal plane.

C. On the transducer axis

On the transducer axis, $Y=2G_p(r_0/z-1)$, and $Z=0$, where z has been used in place of r, we have $v_0(Y,0)=1$, $v_1(Y,0)=0$, and

$$\frac{2}{Y}I(Y,0)=\frac{1-\exp(-iY/2)}{iY/2}$$
$$=\frac{1-\exp[-iG_p(r_0/z-1)]}{iG_p(r_0/z-1)}. \tag{49}$$

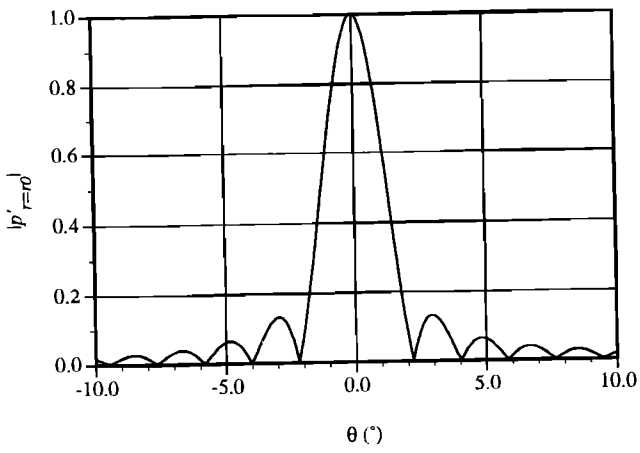

FIG. 4. Normalized pressure distribution on the surface $r=r_0$ for a focused transducer with $\sin\alpha=0.1$ and $ka=100$ ($G_p=5$).

Therefore the normalized pressure distribution is

$$p'_{\text{axial}}=\exp[-ik(z-r_0)]\,\frac{r_0}{z}\,\frac{1-\exp[-iG_p(r_0/z-1)]}{iG_p(r_0/z-1)}, \tag{50}$$

and its amplitude is

$$|p'_{\text{axial}}|=\frac{r_0}{z}\left|\frac{\sin[(G/2)(r_0/z-1)]}{(G/2)(r_0/z-1)}\right|. \tag{51}$$

From Eq. (51) the pressure maximum on the axis occurs at

$$\frac{z_{\max}}{r_0}=1-\frac{12}{G_p^2}+O\left(\frac{1}{G_p^4}\right). \tag{52}$$

This agrees with the result obtained by Lucas and Muir.[6] Substituting (52) into (51), the pressure maximum on the axis is

$$p'_{\max}\approx\left(\frac{G_p}{6}+\frac{2}{G_p}\right)\sin\frac{6}{G_p}>1. \tag{53}$$

Shown in Fig. 5 are the axial pressure distributions as a function of z/r_0 for $\sin\alpha=0.1$ and $ka=100$ ($G_p=5$) and $ka=300$ ($G_p=16$). It is important to notice that beyond the focal point, the pressure amplitude decays faster than $1/z$. For $G_p>2\pi$, pressure amplitude has a finite number of zeroes (pressure nodes) beyond the focal point at

$$\frac{z_n}{r_0}=\frac{1}{1-2n\pi/G_p},\quad n=1,2,\ldots<\frac{G_p}{2\pi}. \tag{54}$$

For $G_p<2\pi$ no such pressure nodes exist.

The axial pressure distribution can be obtained without the use of Fresnel approximation. By letting $\theta=0$ and $r=z$, Eq. (5) becomes

$$r'=[z^2+2zr_0(r_0/z-1)(1-\cos\theta_0)]^{1/2}. \tag{55}$$

Substituting into Eq. (2), and integrating directly, we have

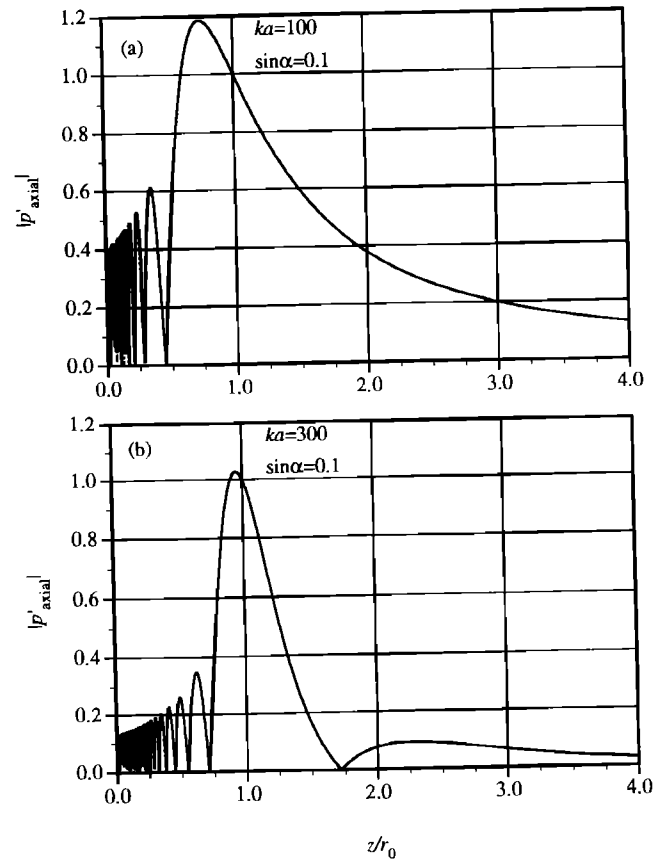

FIG. 5. Normalized axial pressure distribution of a focused transducer with (a) $\sin\alpha=0.1$, $ka=100$ ($G_p=5$); (b) $\sin\alpha=0.1$, $ka=300$ ($G_p=15$). Dashed line represent the exact solution Eq. (58).

$$\phi_{\text{axial}}=\frac{u_0}{ik}\exp(-ikz)\,\frac{r_0}{z}\left[1-\exp\left(-ikz\left\{\left[1+\frac{4r_0}{z}\times\left(\frac{r_0}{z}-1\right)\sin^2\frac{\alpha}{2}\right]^{1/2}-1\right\}\right)\right]\left(\frac{r_0}{z}-1\right)^{-1}. \tag{56}$$

Hence,

$$p_{\text{axial}}=p_0\exp(-ikz)\,\frac{r_0}{z}\left[1-\exp\left(-ikz\left\{\left[1+\frac{4r_0}{z}\times\left(\frac{r_0}{z}-1\right)\sin^2\frac{\alpha}{2}\right]^{1/2}-1\right\}\right)\right]\left(\frac{r_0}{z}-1\right)^{-1} \tag{57}$$

and its amplitude is

$$|p_{\text{axial}}|=\frac{2p_0}{r_0/z-1}\,\frac{r_0}{z}\sin\left(\frac{kz}{2}\left\{\left[1+\frac{4r_0}{z}\left(\frac{r_0}{z}-1\right)\times\sin^2\frac{\alpha}{2}\right]^{1/2}-1\right\}\right). \tag{58}$$

This is the exact solution of the axial pressure distribution and it agrees with the solution by O'Neil.[3] It is easy to show that, for $z>a$, Eq. (58) is reduced to Eq. (51) when normalized by p_0G_p. This can be seen in Fig. 5, where the two equations are shown together. The difference between them is only visible for $z<a$.

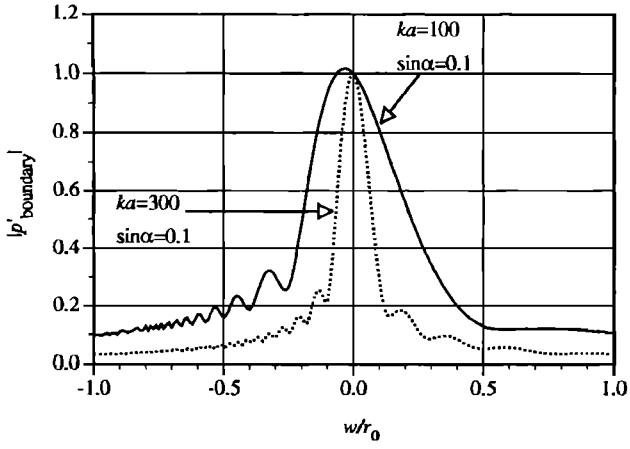

FIG. 6. Normalized pressure distribution on the boundary line for a focused transducer with $\sin\alpha=0.1$, $ka=100$ ($G_p=5$) and $\sin\alpha=0.1$, $ka=300$ ($G_p=15$).

From Eq. (58), the pressure node beyond the focal point is actually located at

$$\frac{z_n'}{r_0}=\frac{1-(2n\pi/ka)^2}{1-2n\pi/G_p}, \quad n=1,2,\ldots<\frac{G_p}{2\pi}. \tag{59}$$

Equation (59) also gives all the zeroes before the focal point where $n=-1,-2,\ldots>-ka/2\pi$.

From Eq. (58), the pressure amplitude at the center of the transducer ($z=0$) is

$$|p_{\text{center}}|=2p_0|\sin(ka/2)|. \tag{60}$$

This indicates that the pressure amplitude at the center of the transducer varies from 0 to $2p_0$ depending on the value of ka. This phenomena has been observed for a flat piston transducer.[9]

D. On the boundary

On the boundary line separating the shadow and illuminated zones, the normalized pressure amplitude can be found from Eqs. (27) and (36) to be

$$p'_{\text{boundary}}=\exp\left[-ikr_0\left(\frac{r}{r_0}-1\pm\frac{a\sin\theta}{2r_0}\right)\right]\times\frac{r_0}{r}\frac{1-\exp(\mp ika\sin\theta)J_0(ka\sin\theta)}{ika\sin\theta} \tag{61}$$

and its amplitude is

$$|p'_{\text{boundary}}|=\frac{r_0}{r}\frac{1}{ka\sin\theta}[1+J_0^2(ka\sin\theta)-2\cos(ka\sin\theta)J_0(ka\sin\theta)]^{1/2}. \tag{62}$$

Let w be the distance measured from the focal point to the observation point along the boundary line, as shown in Fig. 2, then

$$r=(w^2+r_0^2+2wr_0\cos\alpha)^{1/2},\qquad \sin\theta=|w|\sin\alpha/r. \tag{63}$$

Figure 6 shows the pressure distribution along the boundary line for $\sin\alpha=0.1$ and $ka=100$ and 300. From Eq. (62) it can be proven that there are no pressure nodes along the boundary line for any values of ka.

At the edge of the transducer, where $r\approx a$ and $\theta\approx\pi/2$, the pressure amplitude is

$$|p_{\text{edge}}|\approx(p_0/2)[1+J_0^2(ka)-2\cos(ka)J_0(ka)]^{1/2}. \tag{64}$$

This expression indicates that the pressure amplitude at the edge of the transducer is roughly half of the power equivalent average pressure radiated from the transducer. Similar phenomena has been observed for a flat piston transducer.[10]

E. The physical meaning of p_0

Since the pressure near the center of the transducer can be twice the value of p_0, and the pressure at the edge of the transducer is about half the value of p_0, the physical meaning of p_0 is desired. The total transmitted acoustic power can be computed as

$$P=\frac{1}{2\rho_0 c}\iint|p|^2\,dS, \tag{65}$$

where the integral is chosen to be over the focal plane, since an explicit form for the pressure there has been obtained in Eq. (39). After some manipulation, we have

$$P=\pi a^2\frac{p_0^2}{2\rho_0 c}\int_{u=0}^{ka}\frac{2J_1(u)}{u[1-(u/ka)^2]}\,du. \tag{66}$$

For $ka\gg1$, the value of the integral approaches 1, and $P=\pi a^2(p_0^2/2\rho_0 c)$. So p_0 is the power equivalent average pressure over the transducer surface.

F. Near the focal point

Equation (17) or (36) together with Eqs. (21), (27), and (31) can be used to calculated the pressure amplitude for any point in the right half-space. An example is given near the focal point of a transducer with $\sin\alpha=0.1$ and $ka=200$. The three-dimensional plot in Fig. 7 reveals the complicated pressure pattern just before the focal point.

IV. PRESSURE DISTRIBUTION OF A FLAT PISTON TRANSDUCER

The pressure distribution of a flat piston transducer can be obtained from the solution given above as the limiting case when the radius of curvature r_0 is taken as infinity. Then Eq. (15) becomes

$$Y=ka^2/r,\qquad Z=ka\sin\theta, \tag{67}$$

and the solution of the pressure distribution given in Eq. (17) now becomes

$$p(r,\theta)=ip_0\exp(-ikr)I(Y,Z). \tag{68}$$

Now, since $Y/Z=a/r\sin\theta=a/x$, where x is the lateral distance measured from the transducer axis, we have

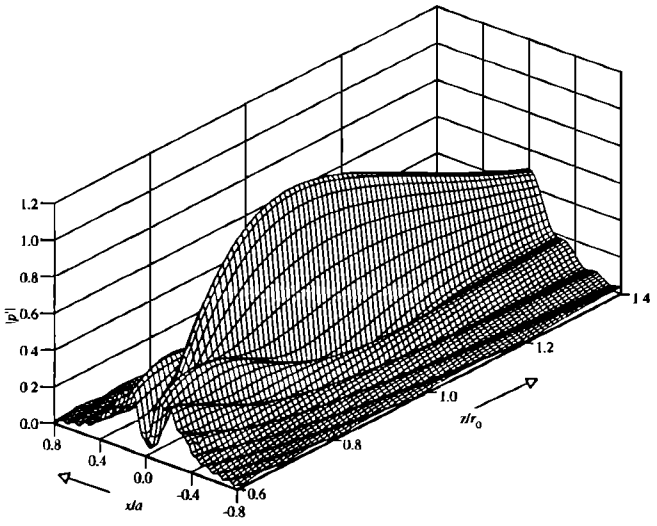

FIG. 7. Normalized pressure distribution near the focal point of a focused traducer with $\sin\alpha=0.1$, $ka=200$.

$$\frac{Y}{Z}=\begin{cases}<1, & \text{shadow zone } (x>a),\\ =1, & \text{boundary } (x=a),\\ >1, & \text{illuminated zone } (x<a).\end{cases} \tag{69}$$

Similar to the solution for the focused transducer, the solution is divided into the shadow zone and the illuminated zone by a boundary line, in this case, $x=a$, as shown in Fig. 8. Equation (21) is used in the shadow zone, Eq. (31) is used in the illuminated zone, and Eq. (27) is used for the boundary line. Many of the radiation field properties discussed by Pierce[9] can be derived from the above formulation.

A. On the transducer axis

On the axis of the transducer, $Z=0$, $v_0=1$, and $v_1=0$. From Eqs. (68) and (31), we have the pressure distribution on the axis of the transducer as

$$p_{\text{axial}}=p_0\exp(-ikz)\left[1-\exp\left(-i\frac{ka^2}{2z}\right)\right], \tag{70}$$

and its amplitude is given by

$$p=2p_0|\sin(ka^2/4z)|. \tag{71}$$

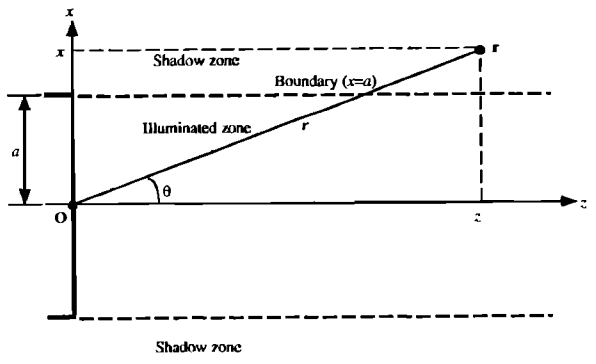

FIG. 8. The definition of illuminated and shadow zones and the boundary line for a flat disk transducer.

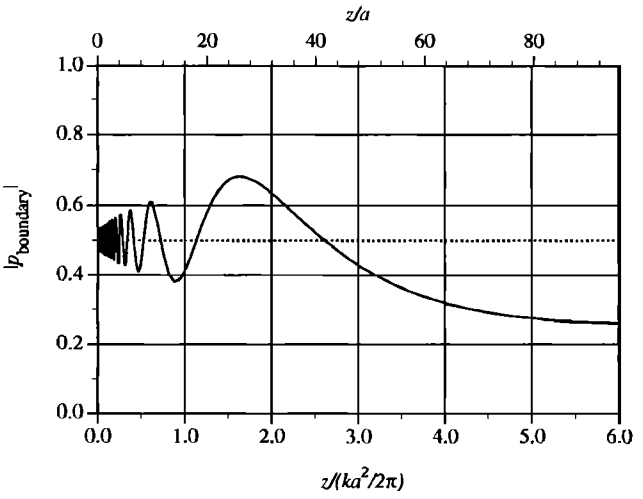

FIG. 9. Pressure distribution along the boundary line $x=a$ as a function of axial distance z normalized by the Rayleigh distance $ka^2/2\pi$, for a flat disk transducer with $ka=100$. Top axis shows the corresponding value of z normalized by a.

The exact solution of the axial pressure distribution can be obtained from Eq. (57) by letting $r_0\to\infty$:

$$p_{\text{axial}}=p_0\exp(-ikz)\times\left\{1-\exp\left[-ikz\left(\sqrt{1+\left(\frac{a}{z}\right)^2}-1\right)\right]\right\}, \tag{72}$$

and its amplitude is

$$|p_{\text{axial}}|=2p_0\sin\left\{\frac{kz}{2}\left[\sqrt{1+\left(\frac{a}{z}\right)^2}-1\right]\right\}. \tag{73}$$

Equation (72) is the exact solution of the axial pressure distribution and agrees with Pierce[9] and Kinsler *et al.*[11] For $z>a$, Eq. (72) reduces to Eq. (70). At the center of the transducer, the pressure amplitude is $|p_{\text{center}}|=2p_0\sin(ka/2)$, the same as for the focused transducer.

B. On the boundary line

The pressure amplitude on the boundary $x=a$ can be found from Eqs. (68) and (27) to be

$$p_{\text{boundary}}=\frac{p_0}{2i}\exp\left[-ikr\left(1-\frac{a\sin\theta}{2r}\right)\right]\times[1-\exp(-ika\sin\theta)J_0(ka\sin\theta)], \tag{74}$$

and its amplitude is

$$|p_{\text{boundary}}|=\frac{p_0}{2}\{1+J_0^2(ka\sin\theta)-2\cos(ka\sin\theta)J_0(ka\sin\theta)\}^{1/2}, \tag{75}$$

where $\sin\theta=a/\sqrt{a^2+z^2}$. Figure 9 shows the pressure distribution along the boundary line for $ka=100$ as a function of z/a.

At the edge of the transducer, where $z=0$, the pressure amplitude is $|p_{\text{edge}}|=(p_0/2)[1+J_0^2(ka)$

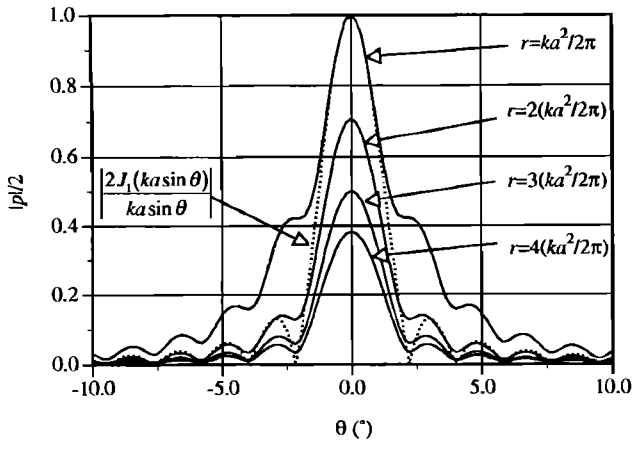

FIG. 10. Angular pressure distribution of a flat disk transducer with $ka=100$ at $r=ka^2/2\pi$, $2(ka^2/2\pi)$, $3(ka^2/2\pi)$, and $4(ka^2/2\pi)$, where $ka^2/2\pi$ is the Rayleigh distance of the transducer. The dashed line represents the function $|2J_1(ka\sin\theta)/ka\sin\theta|$.

$-2\cos(ka)J_0(ka)]^{1/2}$, which is the same as that for a focused transducer and is numerically similar to the solution by Pierce.[9]

C. The far field

When the observation point is far away from the transducer surface ($r\gg ka^2/2\pi$), the pressure distribution becomes relatively simple. The far field can be obtained directly from Eqs. (68) and (23), keeping the first term only:

$$p_{\text{far}}=p_0\exp\left[-ikr\left(1+\frac{a^2}{2r^2}\right)\right]\frac{ka^2}{2r}\frac{2J_1(ka\sin\theta)}{ka\sin\theta}. \quad (76)$$

This is the well-known angular distribution pattern of a flat transducer,[9,12] when the phase correction $-ka^2/2r$ is discarded.

D. Angular distribution

It is import to realize that the far field angular distribution pattern is valid when the distance from the transducer to the observation point is much larger than the Rayleigh distance of the transducer ($ka^2/2\pi$). This fact is demonstrated by Fig. 10, where angular distributions at several locations are shown. Equations (21), (27), and (31) are used with Eq. (68) to calculate these values. The dashed line in Fig. 10 is the function $|2J_1(ka\sin\theta)/ka\sin\theta|$. It is clear that at the Rayleigh distance, the angular distribution function agrees with the far field angular distribution function only within the -3-dB zone, beyond which they diverge drastically. As r gets larger, the angular distribution function approaches the far field value. This is confirmed by Fig. 11, where the pressure distribution near the Rayleigh distance is shown. From Fig. 10, a safe distance beyond which the far field angular distribution pattern can be used is $r>ka^2/2$, i.e., π times the Rayleigh distance.

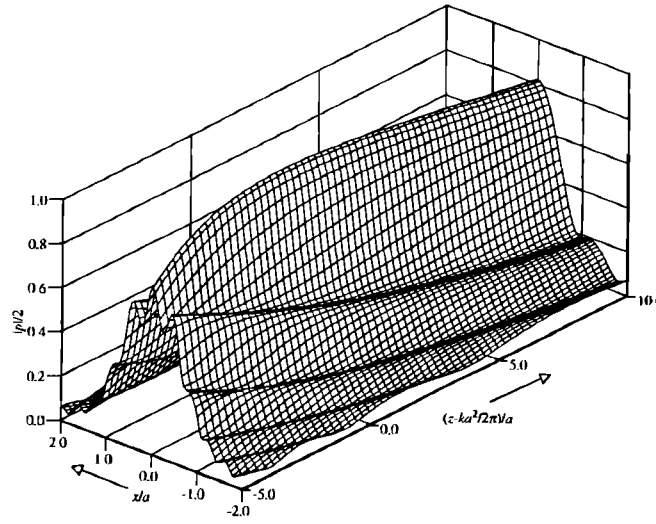

FIG. 11. Pressure distribution of a flat disk transducer with $ka=100$ near the Rayleigh distance.

V. NUMERICAL CONSIDERATIONS

Generally speaking, the computation of Eq. (19), (26), or (30) is needed for the pressure distribution of a focused or flat disk transducer. Since $|J_n(Z)|\leqslant 1$ for any n, the series in Eq. (19) converges faster than

$$\sum_{n=0}^{n=\infty}(-1)^n\left(\frac{Y}{Z}\right)^{2n+1},$$

and the series in Eq. (30) converges faster than

$$\sum_{n=0}^{n=\infty}(-1)^n\left(\frac{Z}{Y}\right)^{2n}.$$

Near the boundary separating the illuminated zone and the shadow zone, where $|Y/Z|\approx 1$, the speed of convergence depends on the value of Z (and hence, Y). When $|Y/Z|\approx 1$ and Z is small in amplitude, the series in both Eqs. (19) and (30) converge rapidly since $J_n(Z)$ is a rapidly decreasing function of n for $n>Z$ and is about equal to $(Z/2)^n$. When $|Y/Z|\approx 1$ and Z (and hence Y) is not small in amplitude, the series in both Eqs. (19) and (30) converge slowly and alternative forms are desired. In this case, the following identities given in the Appendix [Eqs. (A10) and (A11)] are used:

$$\begin{aligned}u_1(Y,Z)=&\frac{1}{2}\left[\sin\left(\frac{Z^2+Y^2}{2Y}\right)-J_0(Y)\sin\left(\frac{Z^2-Y^2}{2Y}\right)\right]\\&-\sum_{n=0}^{n=\infty}(-1)^n\left[J_{2n+1}(Y)\cos E_n\left(\frac{Z^2-Y^2}{2Y}\right)\right.\\&\left.-J_{2n+2}(Y)\sin E_n\left(\frac{Z^2-Y^2}{2Y}\right)\right],\\u_2(Y,Z)=&\frac{1}{2}\left[J_0(Y)\cos\left(\frac{Z^2-Y^2}{2Y}\right)\right.\\&\left.-2J_1(Y)\sin\left(\frac{Z^2-Y^2}{2Y}\right)-\cos\left(\frac{Z^2+Y^2}{2Y}\right)\right]\end{aligned} \quad (77)$$

$$-\sum_{n=0}^{n=\infty}(-1)^n\left[J_{2n+2}(Y)\cos E_n\left(\frac{Z^2-Y^2}{2Y}\right)\right.$$
$$\left.-J_{2n+3}(Y)\sin E_n\left(\frac{Z^2-Y^2}{2Y}\right)\right].$$

where

$$\cos E_n(x)=\cos(x)-\sum_{q=0}^{q=n}(-1)^q\frac{1}{(2q)!}x^{2q},$$
$$\sin E_n(x)=\sin(x)-\sum_{q=0}^{q=n}(-1)^q\frac{1}{(2q+1)!}x^{2q+1}, \tag{78}$$

are the error functions of $\cos(x)$ and $\sin(x)$ when their Taylor expansions are truncated to order n, and an extension of the Bessel functions $J_n(-Y)=(-1)^nJ_n(Y)$ has been used. Notice that both $\cos E_n(x)$ and $\sin E_n(x)$ are decreasing functions of n for $n>|x/2|$. It is easy to show that Eq. (77) reduces to Eq. (26) for $|Y/Z|=1$.

We now specify that for $|Y/Z|\leqslant\sqrt{2}/2$ Eq. (19) will be used, for $|Y/Z|\geqslant\sqrt{2}$ Eq. (30) will be used, and for $\sqrt{2}/2<|Y/Z|<\sqrt{2}$ Eq. (78) will be used. For a focused transducer, this is about equivalent to $\sqrt{2}\alpha\leqslant\theta_1\leqslant\pi-\sqrt{2}\alpha$, $0\leqslant\theta_1\leqslant(\sqrt{2}/2)\alpha$ or $\pi-(\sqrt{2}/2)\alpha\leqslant\theta_1\leqslant\pi$, and $(\sqrt{2}/2)\alpha\leqslant\theta_1\leqslant\sqrt{2}\alpha$ or $\pi-\sqrt{2}\alpha\leqslant\theta_1\leqslant\pi-(\sqrt{2}/2)\alpha$, respectively. For a flat disk transducer, this is equivalent to $\sqrt{2}a\leqslant x\leqslant\infty$, $0\leqslant x\leqslant(\sqrt{2}/2)a$, and $(\sqrt{2}/2)a<x<\sqrt{2}a$, respectively.

The infinite summations $\Sigma_{n=0}^{n=\infty}$ in all these Eqs. are replace by finite summations $\Sigma_{n=0}^{n=N}$, where N is chosen such that the normalized pressure of the focused transducer is calculated to within 0.01 accuracy (-40 dB compared with the pressure amplitude at focus). Since the normalized pressure is proportional to $(2/Y)I(Y,Z)=(2/Y)[u_1(Y,Z)+iu_2(Y,Z)]$, we find N by inspection of the truncation error. The analysis for the flat disk transducer is similar and will be omitted here. For $|Y/Z|\leqslant\sqrt{2}/2$, inspection of Eq. (19) reveals that truncation error is about

$$\varepsilon=\left|\frac{2}{Y}\left(\frac{Y}{Z}\right)^{2N+3}J_{2N+3}(Z)\right|=\left|\frac{2J_{2N+3}(Z)}{Z}\right|\left|\frac{Y}{Z}\right|^{2N+2},$$

and since $|2J_{2N+3}(Z)/Z|<1$, we have $\varepsilon<|Y/Z|^{2N+2}$. For the range of $|Y/Z|$ specified, $\varepsilon<0.008$ for $N=6$. For $|Y/Z|\geqslant\sqrt{2}$, inspection of Eq. (30) reveals that truncation error is about

$$\varepsilon=\left|\frac{2}{Y}\left(\frac{Z}{Y}\right)^{2N+2}J_{2N+2}(Z)\right|=\left|\frac{2J_{2N+2}(Z)}{Z}\right|\left|\frac{Y}{Z}\right|^{2N+3},$$

and since $|2J_{2N+3}(Z)/Z|<1$, we have $\varepsilon<|Z/Y|^{2N+3}$. For the range of $|Y/Z|$ specified, $\varepsilon<0.006$ for $N=6$. For $\sqrt{2}/2\leqslant|Y/Z|\leqslant\sqrt{2}$, inspection of Eq. (78) reveals that truncation error is about

$$\varepsilon=\left|\frac{2}{Y}\frac{1}{(2N+2)!}\left(\frac{Z^2-Y^2}{2Y}\right)^{2N+2}J_{2N+3}(Y)\right|,$$

and since $|J_{2N+3}(Y)|<\sqrt{2/\pi|Y|}$ for $|Y|\gg1$, we have $\varepsilon<[1/\sqrt{\pi}(2N+2)](|Y|/2)^{2N+0.5}$ for the range of $|Y/Z|$ specified. For $|Y|<4\pi$ and $N=7$, we find $\varepsilon<0.01$.

The above discussion is only a rough estimate of terms needed. The actual number of terms needed is much smaller to obtain the degree of precision specified. For example, near the focal plane of a focused transducer and in the far field of a flat transducer, where Y is small in amplitude, $N=0$ is needed to obtain $\varepsilon<0.01$.

Due to the nature of the series solution, recursive method should be used to calculate the values of the Bessel functions, since values of $J_n(Z)$ for roughly $n=0,...,2N+2$ are needed when any of the three solutions are used. Also, since most of the computation time is spent on calculating the values of Bessel functions, it is advised that polar coordinate systems be used. Then for a particular transducer (ka=const), the argument for the Bessel functions is a constant along the line θ=const, and the numerical values of the Bessel functions can be shared along this line.

The use of recursive relations to calculate Bessel functions has been discussed in detail by Abramowitz and Stegun.[13] A brief review is given here for completeness. The recursive relation is given by (Eq. 9.1.27 in Ref. 13)

$$J_{n-1}(Z)+J_{n+1}(Z)=(2n/Z)J_n(Z). \tag{79}$$

We divide Z into two ranges: $0\leqslant Z<3$ and $3\leqslant Z<\infty$. For $0\leqslant Z<3$, we find that $|J_n(Z)|<3\times10^{-8}$ for any $n\geqslant13$. Let $J_{13}(Z)=0$ and $J_{12}(Z)=1$ with an unknown scale factor, then Eq. (79) is used to calculate $J_n(Z)$ for $n=11,10,...,0$. The scale factor is found by using (Eq. 9.1.46 in Ref. 13)

$$1=J_0(Z)+2J_2(Z)+2J_4(Z)+\cdots. \tag{80}$$

For $3\leqslant Z<\infty$, the values of $J_n(Z)$ and $J_1(Z)$ are calculated first by (Eqs. 9.4.3 and 9.4.6 in Ref. 13):

$$J_0(Z)=(1/\sqrt{Z})f_0\cos(\theta_0),$$
$$J_1(Z)=(1/\sqrt{Z})f_1\cos(\theta_1), \tag{81}$$

where f_0, f_1, θ_0, and θ_1 are sixth-order polynomials of $3/Z$ given in Ref. 13. Then Eq. (79) is used to calculate $J_n(Z)$ for $n=2,3,...,2N+2$.

The errors in the calculated Bessel functions are smaller than 1×10^{-7} for both methods.

VI. CONCLUSION

A series solution for the pressure distribution of a focused transducer is presented. The radiation field is divided into two zones: the illuminated zone and the shadow zone. Alternative forms for the pressure distribution are provided. The solution is numerically convergent for any point in the right half-space of the transducer. The pressure on the boundary dividing the different zones is given in an explicit form. This form is most useful for checking the convergence of the series solutions, since they should all provide the same value on the boundary. Near the acoustic axis and far away from the transducer, numerical values of the solution become similar to that given by Lucas and Muir.[6] Near the focal point, numerical values of the solu-

TABLE I. Pressure distribution of focused and flat transducers: Summary of results.

Transducer type	Focused transducer		Flat disk transducer	
Parameters	$Y=\frac{ka^2}{r}\left(1-\frac{r}{r_0}\cos\theta\right)$, $Z=ka\sin\theta$.	Eq. (15)	$Y=ka^2/r$, $Z=ka\sin\theta$.	Eq. (67)
Pressure distribution	$p(r,\theta)=\frac{ip_0\exp(-ikr)}{1-r\cos\theta/r_0}I(Y,Z)$	Eq. (17)	$p(r,\theta)=ip_0\exp(-ikr)I(Y,Z)$.	Eq. (68)
Zones	$\left\|\frac{Y}{Z}\right\|=\begin{cases}<1, & \text{shadow } (\alpha<\theta_1<\pi-\alpha),\\ =1, & \text{boundary } (\theta_1=\alpha \text{ or } \theta_1=\pi-\alpha),\\ >1, & \text{illuminated } (\theta_1<\alpha \text{ or } \theta_1<\pi-\alpha).\end{cases}$	Eq. (25)	$\frac{Y}{Z}=\begin{cases}<1, & \text{shadow } (x>a),\\ =1, & \text{boundary } (x=a),\\ >1, & \text{illiminated } (x<a).\end{cases}$	Eq. (69)
General solution	$I(Y,Z)=Y\int_{u=0}^{1}\exp\left(-i\frac{Y}{2}u^2\right)uJ_0(Zu)du$			Eq. (16)
Shadow zone	$I(Y,Z)=\exp\left(-i\frac{Y}{2}\right)[u_1(Y,Z)+iu_2(Y,Z)]$			Eq. (21)
	$u_1(Y,Z)$, $u_2(Y,Z)$			Eq. (19)
Boundary	$I(\pm Z,Z)=\exp\left(\frac{\pm iZ}{2}\right)\frac{1-\exp(\mp iZ)j_0(Z)}{\pm 2i}$			Eq. (27)
Illuminated zone	$I(Y,Z)=-i\exp\left(\frac{iZ^2}{2Y}\right)\left\{1-\exp\left[-i\left(\frac{Y}{2}+\frac{Z^2}{2Y}\right)\right][v_0(Y,Z)+iv_1(Y,Z)]\right\}$			Eq. (31)
	$v_0(Y,Z)$, $v_1(Y,Z)$			Eq. (30)

tion are similar to that given by Williams.[10] On the acoustic axis, an exact solution is provided, and this solution agrees with that by Williams.[10]

The pressure distribution of a flat disk transducer is obtained as a limiting case of the focused transducer. Graphical presentation indicates that the far field angular distribution function should be used with caution when the distance from the transducer to the observation point is not much larger than the Rayleigh distance.

A summary of the main results is provided in Table I.

Computationally, the series solution given here is more advantageous than the integral solutions. Recursive method should be used to calculate the values of the Bessel functions.

It is only appropriate for us to point out that the mathematical methods used here to derive the acoustic pressure distribution are very similar to the methods used by Born and Wolf,[14] who discussed the light intensity distribution of a focusing lens near the focal point. They defined the following two nondimensional parameters to specify the spatial location of the observer:

$$Y'=\frac{ka^2(z-r_0)}{r_0^2},\quad Z'=kax/r_0. \tag{82}$$

Using their procedures on Eq. (2) for the acoustic case, we find

$$p(r,\theta)=\frac{ip_0\exp(-ikz)}{1-z/r_0}I(Y',Z'). \tag{83}$$

It is now easy to show that the intensity distribution in the neighborhood of the focus is symmetrical about the geometrical focal plane as well as the axis, as Born and Wolf have pointed out.

The parameters Born and Wolf defined are related to the parameters we used by

$$Y'=-Y(r/r_0),\quad Z'=Z(r/r_0). \tag{84}$$

The differences between them are small only near the focus and around the hemispherical surface $r=r_0$. For other locations, we believe our parameters are a better approximation. This can be shown by comparing the phase kr' and its approximation associated with the definition Y and Z. The approximation used by Born and Wolf is intended for the focal area only.

ACKNOWLEDGMENTS

We would like to thank Professor Edwin L. Carstensen of the University of Rochseter for his support of this work. Financial support in part by the National Institute of Health through Grant No. CA44732 and the National Science Foundation through Grant No. EEC9209615 is acknowledged.

APPENDIX: THE COMPUTATION OF LOMMEL FUNCTIONS FOR $|Y/Z|\approx 1$

The general definition of Lommel function of order s is

$$u_s(Y,Z)=\sum_{n=0}^{\infty}(-1)^n\left(\frac{Y}{Z}\right)^{2n+s}J_{2n+s}(Z). \tag{A1}$$

By Taylor's theorem, we have

$$u_s(Y,Z_0+\Delta Z)=\sum_{q=0}^{\infty}\frac{\partial^q u_s(Y,Z_0)}{\partial Z^q}(\Delta Z)^q. \tag{A2}$$

Using the partial derivatives of $u_s(Y,Z)$ given by Gray and Mathews,[8] we have

$$u_s(Y,Z_0+\Delta Z)=\sum_{q=0}^{\infty}(-1)^q\times\frac{(\Delta Z)^q(2Z_0+\Delta Z)^q}{q!(2Y)^q}\times u_{s+q}(Y,Z_0). \tag{A3}$$

Let $Z=Z_0+\Delta Z$, and $Z_0=|Y|$, then $\Delta Z=Z-|Y|$, and Eq. (A3) becomes

$$u_s(Y,Z)=\sum_{q=0}^{\infty}(-1)^q\frac{1}{q!}\left(\frac{Z^2-Y^2}{2Y}\right)^q u_{s+q}(Y,|Y|). \tag{A4}$$

The functions $u_s(Y,|Y|)$ are special cases of Eq. (A1), and can be expressed as

$$u_{2s}(Y,|Y|)=(-1)^s\left(\frac{J_0(Y)+\cos(Y)}{2}-\sum_{n=0}^{n=s-1}(-1)^n J_{2n}(Y)\right),$$
$$u_{2s+1}(Y,|Y|)=(-1)^s\left(\frac{\sin(Y)}{2}-\sum_{n=0}^{n=s-1}(-1)^s J_{2n+1}(Y)\right), \tag{A5}$$

where the natural extension of the Bessel functions of negative argument has been used:

$$J_n(-Y)=(-1)^n J_n(Y). \tag{A6}$$

Equation (A5) is an extension of the results for $u_s(Y,Y)$ given by Gray and Mathews and can be derived from Eq. (26).

Substituting Eq. (A5) into Eq. (A4), and rearranging terms, we have

$$u_{2s+1}(Y,Z)=(-1)^s\left(\frac{\sin(Y)}{2}-\sum_{n=0}^{n=s-1}(-1)^n J_{2n+1}(Y)\right)\cos\left(\frac{Z^2-Y^2}{2Y}\right)+(-1)^s\left(\frac{J_0(Y)+\cos(Y)}{2}-\sum_{n=0}^{n=s}(-1)^n J_{2n}(Y)\right)\sin\left(\frac{Z^2-Y^2}{2Y}\right)-\sum_{n=0}^{n=\infty}(-1)^n\left[J_{2n+2s+1}(Y)\cos E_n\left(\frac{Z^2-Y^2}{2Y}\right)-J_{2n+2s+2}(Y)\sin E_n\left(\frac{Z^2-Y^2}{2Y}\right)\right], \tag{A7}$$

and

$$u_{2s}(Y,Z)=(-1)^s\left(\frac{J_0(Y)+\cos(Y)}{2}-\sum_{n=0}^{n=s-1}(-1)^n J_{2n}(Y)\right)\cos\left(\frac{Z^2-Y^2}{2Y}\right)-(-1)^s\left(\frac{\sin(Y)}{2}-\sum_{n=0}^{n=s-1}(-1)^n J_{2n+1}(Y)\right)\sin\left(\frac{Z^2-Y^2}{2Y}\right)-\sum_{n=0}^{n=\infty}(-1)^n\left[J_{2n+2s}(Y)\cos E_n\left(\frac{Z^2-Y^2}{2Y}\right)-J_{2n+2s+1}(Y)\sin E_n\left(\frac{Z^2-Y^2}{2Y}\right)\right], \tag{A8}$$

where

$$\cos E_n(x)=\cos(x)-\sum_{q=0}^{q=n}(-1)^q\frac{1}{(2q)!}x^{2q},$$
$$\sin E_n(x)=\sin(x)-\sum_{q=0}^{q=n}(-1)^q\frac{1}{(2q+1)!}x^{2q+1} \tag{A9}$$

are the error functions of $\cos(x)$ and $\sin(x)$ when their Taylor expansions are truncated to order n. Equation (26) and the Taylor expansions of $\cos(x)$ and $\sin(x)$ have been used repeatedly to obtain the final form in Eqs. (A7) and (A8).

Let $s=0$ in Eq. (A7) and $s=1$ in Eq. (A8); we have the Lommel functions needed in Sec. V:

$$u_1(Y,Z)=\frac{1}{2}\left[\sin\left(\frac{Z^2+Y^2}{2Y}\right)-J_0(Y)\sin\left(\frac{Z^2-Y^2}{2Y}\right)\right]-\sum_{n=0}^{n=\infty}(-1)^n\times\left[J_{2n+1}(Y)\cos E_n\left(\frac{Z^2-Y^2}{2Y}\right)-J_{2n+2}(Y)\sin E_n\left(\frac{Z^2-Y^2}{2Y}\right)\right], \tag{A10}$$

and

$$u_2(Y,Z)=\frac{1}{2}\left[J_0(Y)\cos\left(\frac{Z^2-Y^2}{2Y}\right)\right.$$
$$-2J_1(Y)\sin\left(\frac{Z^2-Y^2}{2Y}\right)$$
$$\left.-\cos\left(\frac{Z^2+Y^2}{2Y}\right)\right]-\sum_{n=0}^{n=\infty}(-1)^n$$
$$\times\left[J_{2n+2}(Y)\cos E_n\left(\frac{Z^2-Y^2}{2Y}\right)\right.$$
$$\left.-J_{2n+3}(Y)\sin E_n\left(\frac{Z^2-Y^2}{2Y}\right)\right]. \qquad \text{(A11)}$$

[1] P. R. Stepanishen, J. Acoust. Soc. Am. **49**, 841–849 (1971).
[2] J. C. Lockwood and J. G. Willette, J. Acoust. Soc. Am. **53**, 735–741 (1973).
[3] H. T. O'Neil, J. Acoust. Soc. Am. **21**, 516–526 (1949).
[4] A. Penttinen and M. Luukkala, J. Phys. D: Appl. Phys. **9**, 1547–1557 (1976).
[5] E. L. Madsen, M. M. Goddsitt, and J. A. Zagzebski, J. Acoust. Soc. Am. **70**, 1508–1517 (1981).
[6] B. G. Lucas and T. G. Muir, J. Acoust. Soc. Am. **72**, 1289–1296 (1982).
[7] W. N. Cobb, J. Acoust. Soc. Am. **75**, 72–79 (1984).
[8] A. Gray and G. B. Mathews, *A Treatise on Bessel Functions And Their Applications to Physics* (Macmillan, London, 1952), 2nd ed., pp. 178–228.
[9] A. D. Pierce, *Acoustics* (Acoustical Society of America, Woodbury, NY, 1989), Ch. 4.
[10] A. O. Williams, Jr., J. Acoust. Soc. Am. **23**, 1–6 (1951).
[11] L. E. Kinsler, A. R. Frey, A. B. Coppens, and J. V. Sanders, *Fundamentals of Acoustics* (Wiley, New York, 1982), 3rd ed., pp. 176–182.
[12] P. M. Morse and K. U. Ingard, *Theoretical Acoustics* (Princeton U.P., Princeton, NJ, 1986), 1st ed.
[13] M. Abramowitz and I. A. Stegun, *Handbook of Mathematical Functions* (Dover, New York, 1965), pp. 355–386.
[14] M. Born and E. Wolf, *Principles of Optics* (Pergamon, Oxford, 1980), 6th ed., Ch. 8.